

See discussions, stats, and author profiles for this publication at: <https://www.researchgate.net/publication/13812859>

# A flavodoxin that is required for enzyme activation: The structure of oxidized flavodoxin from Escherichia coli at 1.8 Å resolution

ARTICLE *in* PROTEIN SCIENCE · DECEMBER 2008

Impact Factor: 2.85 · DOI: 10.1002/pro.5560061205 · Source: PubMed

---

CITATIONS

45

---

READS

25

## 2 AUTHORS, INCLUDING:



David Hoover

National Institutes of Health

31 PUBLICATIONS 2,763 CITATIONS

[SEE PROFILE](#)

# A flavodoxin that is required for enzyme activation: The structure of oxidized flavodoxin from *Escherichia coli* at 1.8 Å resolution

DAVID M. HOOVER<sup>1</sup> AND MARTHA L. LUDWIG<sup>1,2</sup>

<sup>1</sup>Department of Biological Chemistry, The University of Michigan, Ann Arbor, Michigan 48109

<sup>2</sup>Biophysics Research Division, The University of Michigan, Ann Arbor, Michigan 48109-1055

(RECEIVED May 19, 1997; ACCEPTED August 28, 1997)

## Abstract

In *Escherichia coli*, flavodoxin is the physiological electron donor for the reductive activation of the enzymes pyruvate formate-lyase, anaerobic ribonucleotide reductase, and B<sub>12</sub>-dependent methionine synthase. As a basis for studies of the interactions of flavodoxin with methionine synthase, crystal structures of orthorhombic and trigonal forms of oxidized recombinant flavodoxin from *E. coli* have been determined. The orthorhombic form (space group P2<sub>1</sub>2<sub>1</sub>2<sub>1</sub>,  $a = 126.4$ ,  $b = 41.10$ ,  $c = 69.15$  Å, with two molecules per asymmetric unit) was solved initially by molecular replacement at a resolution of 3.0 Å, using coordinates from the structure of the flavodoxin from *Synechococcus* PCC 7942 (*Anacystis nidulans*). Data extending to 1.8-Å resolution were collected at 140 K and the structure was refined to an  $R_{work}$  of 0.196 and an  $R_{free}$  of 0.250 for reflections with  $I > 0$ . The final model contains 3,224 non-hydrogen atoms per asymmetric unit, including 62 flavin mononucleotide (FMN) atoms, 354 water molecules, four calcium ions, four sodium ions, two chloride ions, and two Bis-Tris buffer molecules. The structure of the protein in the trigonal form (space group P312,  $a = 78.83$ ,  $c = 52.07$  Å) was solved by molecular replacement using the coordinates from the orthorhombic structure, and was refined with all data from 10.0 to 2.6 Å ( $R = 0.191$ ;  $R_{free} = 0.249$ ). The sequence Tyr 58–Tyr 59, in a bend near the FMN, has so far been found only in the flavodoxins from *E. coli* and *Haemophilus influenzae*, and may be important in interactions of flavodoxin with its partners in activation reactions. The tyrosine residues in this bend are influenced by intermolecular contacts and adopt different orientations in the two crystal forms. Structural comparisons with flavodoxins from *Synechococcus* PCC 7942 and *Anabaena* PCC 7120 suggest other residues that may also be critical for recognition by methionine synthase.

**Keywords:** cryocrystallography; electron transfer; *Escherichia coli*; flavodoxin; reductive activation; X-ray structure

Flavodoxins are small flavin mononucleotide-containing proteins found in many microorganisms, where they serve to transfer electrons at low oxidation-reduction potentials. The FMN is bound tightly but noncovalently to a single polypeptide chain, and its one-electron redox potentials are shifted substantially in the presence of the apoprotein so that reduction occurs in two discrete one-electron steps. Among known flavodoxins, the oxidized/semiquinone potentials vary from –50 to –260 mV, whereas potentials for the hydroquinone/semiquinone couple are in the range

–373 to –520 mV. It is the latter equilibrium that is thought to be physiologically important, because most electron-transfer reactions involving flavodoxins occur at low potentials (Mayhew & Ludwig, 1975; Mayhew & Tollin, 1992).

Flavodoxins act as redox mediators in the metabolism of pyruvate, hydrogen, nitrogen, sulfite, and pyridine nucleotides, transferring the reducing equivalents that are essential in these metabolic pathways. In some electron transfer reactions, such as those involving ferredoxin-NADP<sup>+</sup>-reductase, flavodoxins are functionally interchangeable with ferredoxins, and can substitute for ferredoxins under iron-limiting conditions (Mayhew & Tollin, 1992). Other reactions are specific for flavodoxin and display species selectivity. For example, flavodoxin appears to be the obligate electron donor to the iron protein of nitrogenase in *Klebsiella pneumoniae*, because *nif F* (flavodoxin) mutants are unable to support nitrogen fixation (Nieva-Gomez et al., 1980; Shah et al., 1983). Detailed studies of the reactions of flavodoxins with the nitrogenase from *K. pneumoniae* show that heterologous flavodox-

Reprint requests to: Martha L. Ludwig, Biophysics Research Division, University of Michigan, 3038 Chemistry Building, 930 N. University Avenue, Ann Arbor, Michigan 48109-1055; e-mail: ludwig@norway.biop.umich.edu.

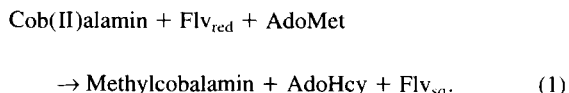
**Abbreviations:** AdoHcy, S-adenosylhomocysteine; DTT, dithiothreitol; FMN, flavin mononucleotide; FNR, ferredoxin/flavodoxin-NADP<sup>+</sup>-reductase; NCS, noncrystallographic symmetry; PFL, pyruvate formate-lyase; RR, ribonucleotide reductase; ox, sq, hq for the FMN oxidation states: oxidized, semiquinone, and hydroquinone.

ins are less efficient than *K. pneumoniae* flavodoxin in reduction of acetylene to ethane (Thorneley & Deistung, 1988). The effectiveness of various flavodoxins as electron donors in this system depends on both redox potential (Deistung et al., 1985) and the ability to form molecular complexes (Thorneley & Deistung, 1988). The three flavodoxins from *Azotobacter vinelandii* (Klugkist et al., 1986) differ in their efficiencies as donors to nitrogenase and nitrate reductase (Gangeshwaran & Eady, 1996). Thus, there are ample precedents for selective interactions of flavodoxin in electron-transfer reactions.

Flavodoxins play a special role in several enzyme activation systems, where they are the required electron donors in essential priming or reactivation reactions. Flavodoxin-dependent activations have been studied most thoroughly in *Escherichia coli*, where flavodoxin provides reducing equivalents for the generation of protein radical intermediates in two key anaerobic enzymes, pyruvate formate-lyase (Vetter & Knappe, 1971; Blaschkowski et al., 1982) and anaerobic ribonucleotide reductase (Bianchi et al., 1993a). In these systems, AdoMet is converted to a 5'-deoxyadenosyl radical and methionine by flavodoxin and activating enzymes, and the 5'-deoxyadenosyl radical in turn abstracts a backbone  $\alpha$ -hydrogen from PFL or ribonucleotide reductase to form a glycyl radical. The activating enzymes for PFL (Wong et al., 1993) and RR (Sun et al., 1995) appear to be [4Fe-4S] proteins in which a reduced iron-sulfur cluster reacts with AdoMet to generate the 5'-deoxyAdo radical (Ollagnier et al., 1997). The activity of biotin synthase may also depend on an analogous flavodoxin-dependent activation (Ifuku et al., 1994; Birch et al., 1995; Sanyal et al., 1996). Ferredoxin cannot replace flavodoxin in the PFL activation reaction (Blaschkowski et al., 1982), suggesting that other activation reactions may also be specific for flavodoxin. The constitutive expression of flavodoxin at low levels in *E. coli* is important for these reactions.

Our focus has been on the role of *E. coli* flavodoxin in the activation of methionine synthase. In contrast to the PFL and ribonucleotide reductase reactions, activation of cobalamin-dependent methionine synthase by AdoMet and reduced flavodoxin (Fujii & Huennekens, 1974) does not involve formation of the 5'-deoxyAdo radical, but instead is a reductive methylation of the inactive cob(II)alamin form of methionine synthase, as shown in Figure 1 and

Equation 1:



The inactive cob(II)alamin form of methionine synthase is generated occasionally (once every 100–1,000 reaction cycles) by oxidation of the reactive cob(I)alamin intermediate that forms when the methyl group of methylcobalamin is transferred to homocysteine. As written, Equation 1 assumes that fully reduced flavodoxin is the reductant, but *in vitro* the reactivation of methionine synthase can also utilize the flavodoxin semiquinone as the electron donor species (Fujii et al., 1977); irreversibility of the methylation by AdoMet drives the overall reaction (Banerjee et al., 1990).

The interaction of *E. coli* flavodoxin with methionine synthase in its cob(II)alamin form, the substrate for reactivation, is accompanied by functionally important structural changes (Hoover et al., 1997). Binding of flavodoxin is manifested by changes in the EPR spectrum of the B<sub>12</sub> cofactor that signal dissociation of the histidine ligand, His 759, from the cobalt, and is accompanied by the uptake of a proton (Hoover et al., 1997). Studies of the His 759 Gly and Asp 757 Glu mutants (Jarrett et al., 1996) have shown that dissociation of the histidine ligand facilitates reductive methylation by AdoMet. At comparable concentrations, the heterologous flavodoxin from *Synechococcus* 7942 does not elicit the characteristic spectral changes in methionine synthase, and *Synechococcus* flavodoxin apparently binds methionine synthase more weakly, by a factor of at least 100, than does *E. coli* flavodoxin (Hoover et al., 1997). Our hypothesis has been that the selective binding of *E. coli* flavodoxin stabilizes a conformation of methionine synthase in which the cobalamin cofactor and bound AdoMet are brought close together for methyl transfer (Drennan et al., 1997; Ludwig & Matthews, 1997). Binding of flavodoxin produces changes in the pattern of tryptic digestion of methionine synthase, indicating alterations in the accessibilities of cleavage sites (Huang & Matthews, 1997). As a basis for studies of the specific interactions between *E. coli* flavodoxin and methionine synthase, structures of two crystal forms of *E. coli* flavodoxin have been determined. One form has been refined with data extending to 1.8 Å resolution and the other with data to 2.6 Å.

## Results and discussion

### Overall structure: Comparisons with other flavodoxins

Although *E. coli* flavodoxin interacts selectively with its acceptors in activation systems, the polypeptide fold of this flavodoxin is quite similar to several other “long-chain” flavodoxins that are 170–180 residues in length (Figs. 2, 3; Table 1). All flavodoxins are  $\alpha/\beta$  proteins with five parallel beta strands flanked on both sides by helices. In the long-chain flavodoxins, the final strand is broken into two sections by an insertion of approximately 20 residues, and the insert itself is organized around a small antiparallel sheet. The secondary structures in crystalline *E. coli* flavodoxin, assigned according to the algorithm of Kabsch and Sander (1983), can be seen in Figure 2 and are diagrammed in Figure 3. In addition to the four long helices, a short helix is found before the start of  $\beta$ -strand 3 in *E. coli* and most other flavodoxins. Hydrogen bonded residues that comprise the small antiparallel sheet in the

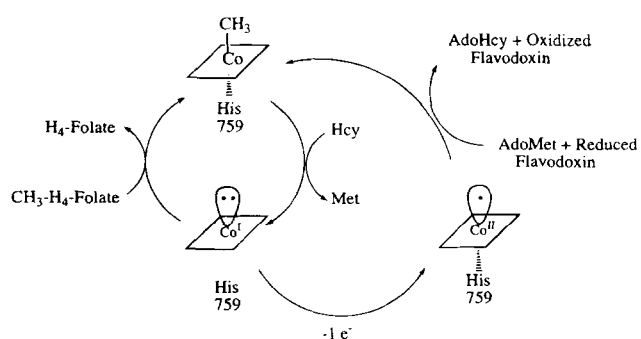


**Fig. 1.** Catalytic and activation cycles of methionine synthase. In the catalytic cycle, shown in the upper left, the methyl group of methyltetrahydrofolate is transferred to homocysteine via the intermediate methylcobalamin, and the cobalamin cofactor alternates between the methylcobalamin and cob(I) alamin forms. One-electron oxidation of the cob(I)alamin form, shown in the lower right, inactivates methionine synthase. The reductive methylation that utilizes reduced flavodoxin as an electron donor reactivates the enzyme and is essential to maintain methionine synthesis.

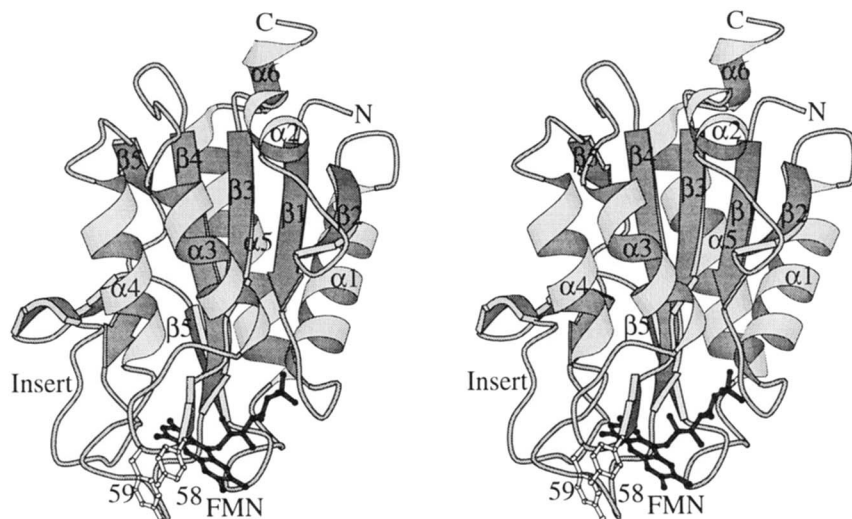


**Fig. 2.** Ribbon drawing of *E. coli* flavodoxin (Kraulis, 1991). The five central parallel  $\beta$ -strands, represented as arrows, are covered by the major helices ( $\alpha_1$ ,  $\alpha_3$ ,  $\alpha_4$ ,  $\alpha_5$ ). A small antiparallel sheet (on the left) is formed by residues from the insert that breaks strand five of the parallel sheet, and a short helix at residues 41–45 ( $\alpha_2$ ) precedes  $\beta_3$ . The helical portion of the C-terminal tail can be seen at the top of the drawing. Residues that contribute to secondary structures are identified in Figure 3.

insert are at positions 120–121, 133–135, and 138–139, and an antiparallel hairpin beneath the flavin is formed by hydrogen-bonding of residues 56–57 and 60–61. The C-terminus of *E. coli* flavodoxin extends for an extra seven residues beyond the termini found in the structures of *Synechococcus* 7942 or *Anabaena* 7120 flavodoxins. The first part of this C-terminal extension has been modeled as a short helix that lies across the “top” of the molecule (Fig. 2) and appears to be stabilized by a hydrophobic cluster involving Leu 168, Leu 170, Ile 173, Leu 174, and residues from the N-terminal end of the  $\beta$ -sheet. This helix is not well-ordered, as indicated by its large temperature factors, and the following two residues are difficult to place in the electron density.

Recent NMR studies of *E. coli* flavodoxin have assigned the  $^1\text{H}$ ,  $^{15}\text{N}$ , and  $^{13}\text{C}$  resonances and permitted the independent determination of the secondary structure of the molecule in solution (Ponstingl & Otting, 1997). Overall, there is good correspondence of the secondary structures observed in the crystal and in solution. Assignments made from X-ray coordinates according to Kabsch and Sander (1983) tend to trim residues at the ends of helices or sheet strands when they are not fully hydrogen bonded, whereas some of these residues are retained in the NMR assignments. Thus, in the NMR analysis, parallel  $\beta$ -strands are extended by inclusion of residues 9, 30, 81, 89, and 117, and residues 13, 46, and 74 are added to helices. The NMR studies did not fully identify the small  $\beta$ -sheet in the insert or the short antiparallel hairpin near the flavin at residues 56–57 and 61–62; residues 57, 90, and 143–144 were assigned to parallel sheet strands by Ponstingl and Otting (1997), but do not make sheet hydrogen bonds in the X-ray structure. The largest difference between the crystal and solution studies seems to be the absence of NMR evidence for the short C-terminal helix, which may be destabilized in solution.

#### The FMN binding site: Comparisons with other flavodoxins

Flavodoxins bind FMN very tightly.  $K_d$  values at pH 7.0 are typically 1–10 nM; the  $K_d$  for *E. coli* flavodoxin, reported here, is

1 nM. Polypeptide segments connecting secondary structural elements are involved in binding the isoalloxazine ring and phosphate group of the FMN cofactor; three regions of the protein sequence account for most of the FMN–protein contacts. The conserved sequence in the loop between  $\beta_1$  and  $\alpha_1$  (Ser<sup>10</sup>·Asp·Thr·Gly·Asn·Thr<sup>15</sup> in *E. coli* flavodoxin) makes a number of N-H···O and O-H···O hydrogen bonds to phosphate oxygens of the cofactor. The conformation of this loop is the most invariant feature of the flavodoxin fold. Hydrogen bonding to the backbone atoms of residues in the 50's and 90's loops and packing against the side chains of the conserved aromatic residues Trp 57 and Tyr 94 hold the isoalloxazine ring in place. The predominance of hydrogen bonding to the peptide backbone is striking (Table 2) and is a general feature of the known flavodoxin structures. In oxidized *E. coli* flavodoxin, the pyrimidine end of the isoalloxazine ring hydrogen bonds to backbone atoms of residues 60, 90, 97, and 99 (Table 2; Fig. 4). Analyses of binding interactions have concentrated on modifying the FMN rather than on residue replacements in the protein (reviewed in Mayhew & Tollin, 1992). However, the tyrosine residue that stacks against the outer surface of the flavin ring in *Desulfovibrio vulgaris* flavodoxin has been replaced by several other residues; substitution by alanine decreases the association constant by a factor of 10 (Swenson & Krey, 1994; Zhou & Swenson, 1996).

The length and conformation of the 50's loop varies among flavodoxins (see Fig. 3), and the interactions of this part of the polypeptide with the isoalloxazine ring are species-dependent (Ludwig & Luschinsky, 1992). The 50's loops in the short-chain flavodoxins from *Clostridium beijerinckii* and *Megasphaera elsdenii* resemble one another closely, but in the short chain of *D. vulgaris* flavodoxin, the 50's loop is longer and oriented differently relative to the isoalloxazine ring. The long-chain flavodoxin from *Chondrus crispus* has four extra residues in the 50's loop, and adopts a novel structure in this region. Although the backbone of *E. coli* flavodoxin differs from the short-chain and *C. crispus* flavodoxins at residues 57–61, it is very similar to flavodoxins from *Synecho-*

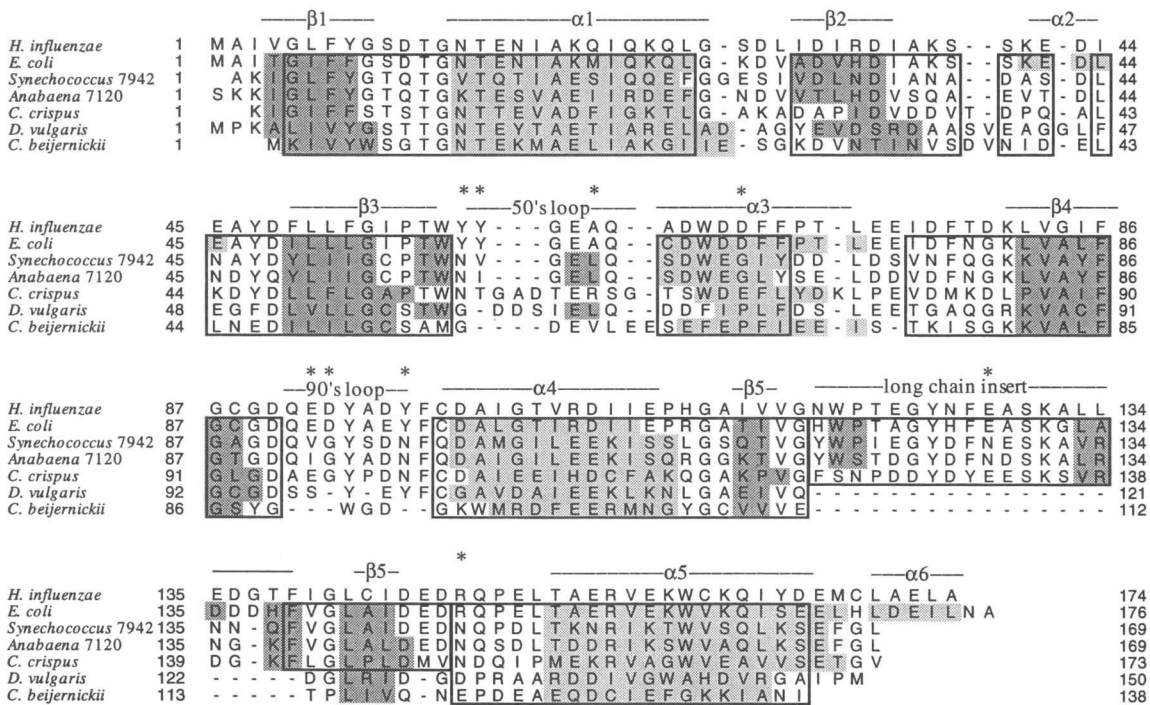


**Fig. 3.** Alignment of flavodoxin sequences. Sequences from *H. influenzae* (Fleischmann et al., 1995), *E. coli* (Osborne et al., 1991), *Anabaena* sp. PCC 7120 (Fillat et al., 1988), *Synechococcus* sp. PCC 7942 (Laudenbach et al., 1988), *C. crispus* (Wakabayashi et al., 1989), *D. vulgaris* (Krey et al., 1988), and *C. beijerinckii* (Tanaka et al., 1974) were aligned using the X-ray structures (this work; Watengaugh et al., 1973; Burnett et al., 1974; Smith et al., 1983; Fukuyama et al., 1990; Burkhardt et al., 1995). PDB filecodes are 1ag9, 1ref, 10fv, 2fer, 2fx2, and 3fxn, respectively. Boxes denote regions in which backbones superimposed with RMSDs < 1.8 Å. Alignments of the sequences between the boxes are essentially those found by sequence-matching algorithms, and do not attempt to indicate which residues occupy similar positions in space. Darker shading designates  $\beta$ -strands and lighter shading designates helices. Secondary structures were assigned to *E. coli* flavodoxin using DSSP (Kabsch & Sander, 1983). The antiparallel sheet in the insert, formed by residues 120–121, 133–135, and 138–139 in *E. coli* flavodoxin, includes a bulge that accommodates an extra residue in the *E. coli* sequence. Asterisks denote the residues that may be important in the interaction with methionine synthase (see text and Table 3).

*coccus* 7942 (Drennan, 1995) and *Anabaena* 7120 (Burkhardt et al., 1995) (Fig. 4).

The contacts between the 90's loop and the flavin ring also vary from species to species. An aromatic residue covers the outer

**Table 1.** Comparison of *E. coli* with other flavodoxins: Backbone RMSDs and sequence identities

	RMSD <sup>a</sup> (Å)	Percent identity <sup>b</sup>
<i>E. coli</i>	(0.220) <sup>c</sup>	100
<i>E. coli</i>	0.427 <sup>d</sup>	100
<i>Anabaena</i> PCC 7120	0.736	46.7
<i>Synechococcus</i> PCC 7942	0.745	48.9
<i>C. crispus</i>	1.329	39.4
<i>D. vulgaris</i>	2.407	37.1
<i>C. beijerinckii</i>	2.883	25.7

<sup>a</sup>Calculated for the equivalent residues that are enclosed in boxes in Figure 3.

<sup>b</sup>Based on the alignment in Figure 3.

<sup>c</sup>RMSD between the NCS-related molecules of the orthorhombic form.

<sup>d</sup>RMSD between molecule 1 of the orthorhombic form and the trigonal form.

surface of the flavin ring, but there are two different backbone motifs. In all flavodoxins except those from *C. beijerinckii* and *M. elsdenii*, the 90's sequence folds over the outer (*si*) side of the FMN ring and forms backbone hydrogen bonds to the NH(3) and O(2) of the isoalloxazine. The 90's loop is much shorter in *C. beijerinckii* and *M. elsdenii* flavodoxins, and the NH(3) of the isoalloxazine is hydrogen bonded to the side chain of a glutamate in the 50's loop.

#### Oxidation-reduction potentials

Residues in the 50's and 90's loops play an important role in control of FMN midpoint potentials in flavodoxins (Ludwig & Luschinsky, 1992; Swenson & Krey, 1994; Mayhew et al., 1996; Ludwig et al., 1997). Variations in the amino acid sequences of the 50's loops have an impact on the redox potentials of flavodoxins even when the backbones are very similar (Ludwig et al., 1997). The oxidized/semiquinone midpoint potential for *E. coli* flavodoxin is –240 to –260 mV versus SHE (Vetter & Knappe, 1971; Hoover, 1997), below that of free FMN (Draper & Ingraham, 1968), and is the lowest ox/sq potential observed for any wild-type flavodoxin. The corresponding midpoint potentials for *Synechococcus* 7942 and *Anabaena* 7120 flavodoxins are –221 and –196 mV, respectively. Studies of *C. beijerinckii* flavodoxin mutants, in which the residue analogous to position 58 in *E. coli* flavodoxin

**Table 2.** Polar contacts between FMN and apoflavodoxin

FMN atom	Protein or solvent atom	Distance, mol 1 (Å)	Distance, mol 2 (Å)	Distance, trigonal (Å)
N1	N90	3.1	3.0	3.2
O2	N90	3.4	3.4	3.0
	N99	3.0	3.0	3.3
N3	O97	2.9	2.8	3.3
O4	N59 <sup>a</sup>	3.2	3.1	3.2
	N60	2.8	2.8	3.0
N5	N58	3.4	3.5	3.2
O2*	O56	2.6	2.7	2.6
O3*	OD2 147	2.8	2.8	2.7
	Wat	2.9 (O <sub>509</sub> )	2.6 (O <sub>452</sub> )	2.7 (O <sub>236</sub> )
O4*	OD1 14	3.0	2.8	3.0
	Wat	2.9 (O <sub>524</sub> )	2.6 (O <sub>503</sub> )	2.8 (O <sub>186</sub> )
OP1	OG1 12	2.7	2.9	2.7
	N14	2.8	2.7	3.2
OP2	NE1 57	2.8	2.9	2.7
	N11	2.8	2.8	2.8
	N12	3.2	3.3	3.4
OP3	OG 10	2.7	2.8	2.7
	OG1 15	2.9	2.8	2.9
	N15	2.9	2.9	2.8

<sup>a</sup>The NH···O angle is smaller than expected for hydrogen bonding.

was mutated from glycine to increasingly bulkier side chains (Ludwig et al., 1997), have shown that this side chain influences redox potentials by altering the energy associated with backbone rearrangements that accompany reduction to the semiquinone. A tyrosine residue at this critical position would be expected to exert a large effect on the energetics of rearrangement, but we do not yet know whether the backbone rearrangement occurs in *E. coli* flavodoxin. The presence of Ca<sup>2+</sup> (see below) has complicated attempts to reduce the crystals for structure analyses.

The potential for the semiquinone/hydroquinone couple in *E. coli* flavodoxin, -440 to -455 mV at pH 7 (Vetter & Knappe, 1971; Hoover, 1997), is typical for flavodoxins. In many flavodoxins, including the flavodoxin from *Anabaena* 7120 that resembles *E. coli* flavodoxin, <sup>15</sup>N chemical shifts of the flavin N(1) atom indicate that N(1) is not protonated in the hydroquinone state (Francken et al., 1984; Stockman et al., 1988). Thus, the reduced isoalloxazine bound to flavodoxins is anionic, and the low sq/hq potential can be attributed to unfavorable electrostatic interactions between the negatively charged flavin and its protein environment (Ludwig et al., 1990; Swenson & Krey, 1994; Zhou & Swenson, 1995, 1996). In *E. coli* flavodoxin, Tyr 58 and Tyr 59, along with Tyr 94, Tyr 97, and Trp 57, provide a hydrophobic shell that shields the flavin ring from solvent (Fig. 4). Solvent exclusion is expected to lower the effective dielectric constant and may thereby destabilize the negatively charged flavin hydroquinone (Swenson & Krey, 1994).

#### Structural waters in *E. coli* flavodoxin

Several waters with small temperature factors and multiple protein contacts appear to play a structural role in long-chain flavodoxins (Hoover, 1997). In *E. coli* flavodoxin, one of these waters (W511)

is located near NH85, and provides a hydrogen bonded bridge between β strands 4 and 5 at the beginning of the insertion in strand 5. Another water (W524) hydrogen bonds to NH146, O89, and the ribityl O4\*. A third buried water (W451) is located near NH145 and Arg 156 in the crystal structure, and a fourth (W505) interacts with the backbone oxygens of Ile 54 and Cys 88. The first three of these bound waters were detected by analysis of water–flavodoxin NOEs (Ponstingl & Otting 1997) and were located with reference to the model structure of Havel (1993).

#### Calcium Bis-Tris, and other ions in the crystal structures of *E. coli* flavodoxin

Calcium ions bridge the molecules that are related by noncrystallographic symmetry in the orthorhombic structure, and display approximate octahedral coordination to protein and water oxygens (Fig. 5). Two chloride ions and four sodium ions (see Materials and methods) are also associated with this intermolecular bridge, which lies near the flavin rings. In addition, two other regions of nonprotein density, near helix α1 and preceding helix α5, have been modeled as Bis-Tris molecules liganded to calcium ions. Bis-Tris ligates calcium well in solution (Good et al., 1966), and these complexes connect crystallographically related molecules, further stabilizing the orthorhombic crystal form. The calcium in the Bis-Tris complex is seen to be liganded by seven, rather than six, oxygen atoms, with a close contact to the tertiary nitrogen of the Bis-Tris molecule that forces the calcium into a distorted coordination geometry. The orthorhombic crystals grow only in the presence of Bis-Tris buffer, whereas the choice of buffer has little effect on the growth of the trigonal crystals. Calcium is required for the growth of the trigonal crystals, and calcium also bridges crystallographically related monomers in the trigonal crystal form. However, the calcium ions are not bound in the same way as in the orthorhombic structure. They connect backbone carbonyl oxygens of residues 148 from one molecule and 93 from the neighbor, stabilizing an intermolecular contact not found in the orthorhombic crystal form.

#### Comparisons of the orthorhombic and trigonal crystal forms of *E. coli* flavodoxin

The trigonal crystal form was obtained in the absence of Bis-Tris buffer. This form has a smaller unit cell, with one molecule per asymmetric unit, and large crystals diffract to higher resolution than the orthorhombic form, but are highly twinned. The untwinned crystal used for data collection was small and intensities were measured only to 2.6 Å resolution. The structure was solved by molecular replacement, using the refined model from the orthorhombic crystal. Rotation and translation searches gave an unambiguous peak, and the refinement was straightforward (see Materials and methods).

The most significant differences between the proteins in the orthorhombic and trigonal crystals are near the FMN binding site. In both structures, tyrosines 58 and 59 provide key contacts for the crystal packing, but the intermolecular packing is somewhat altered and the side chains of tyrosines 58 and 59 adopt different orientations (Fig. 4). The ring of Tyr 59 makes edge to face contacts with Tyr 58 in the orthorhombic structure, whereas, in the trigonal structure, Tyr 58 contacts Trp 57 and Tyr 59 moves toward the former position of the Tyr 58 ring. Comparisons of the two

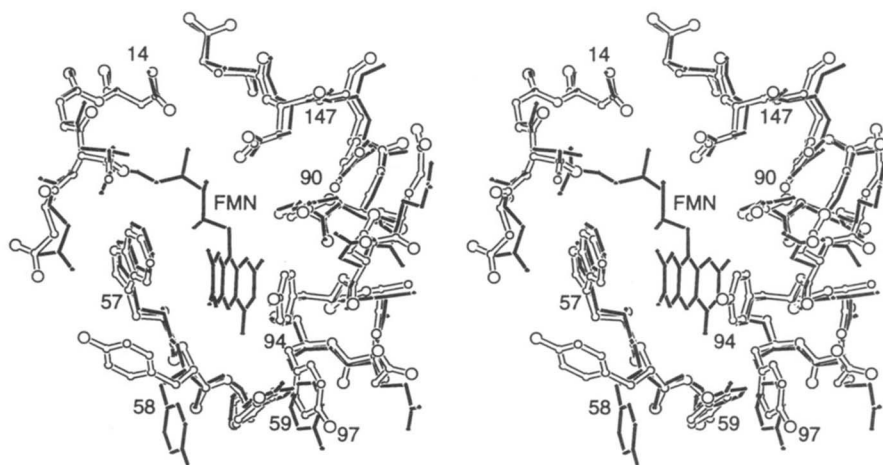


**Fig. 4.** Flavin binding site in *E. coli* flavodoxin. This stereo drawing shows the five aromatic residues that surround the FMN in *E. coli* flavodoxin (Trp 57, Tyr 58, Tyr 59, Tyr 94, and Tyr 97), as well as other residues that make close contacts with the cofactor. The orthorhombic structure is shown in solid bonds, and the trigonal structure is shown in open bonds. Except for Tyr 58, side chains occupy very similar positions in both structures. In the trigonal crystal form, Tyr 58 rotates to contact Trp 57. This rearrangement allows tyrosine 59 to move nearer to the former position of tyrosine 58. The drawing was prepared with the program MAXIM, written by M. Rould.

structures suggest that these side chains are mobile, as predicted by Havel (1993).

In the trigonal crystals, cysteine 64, which is 6 Å from the dimethyl end of the flavin ring, makes a disulfide bond with its crystallographically related mate. Formation of this crosslink appears to be critical in packing of the trigonal crystal form. The growth of trigonal crystals is inhibited by the presence of reduced

DTT, although the crystals themselves are not shattered by addition of DTT. The disulfide can be formed in solution, and its formation is accelerated in the presence of calcium, or in alkaline and mildly denaturing conditions. In solution, the S-S bond is broken by incubation with reduced DTT. A similar situation exists for the flavodoxin from *A. vinelandii*, where the corresponding cysteine, Cys 69, can form an intermolecular disulfide. The dimer-

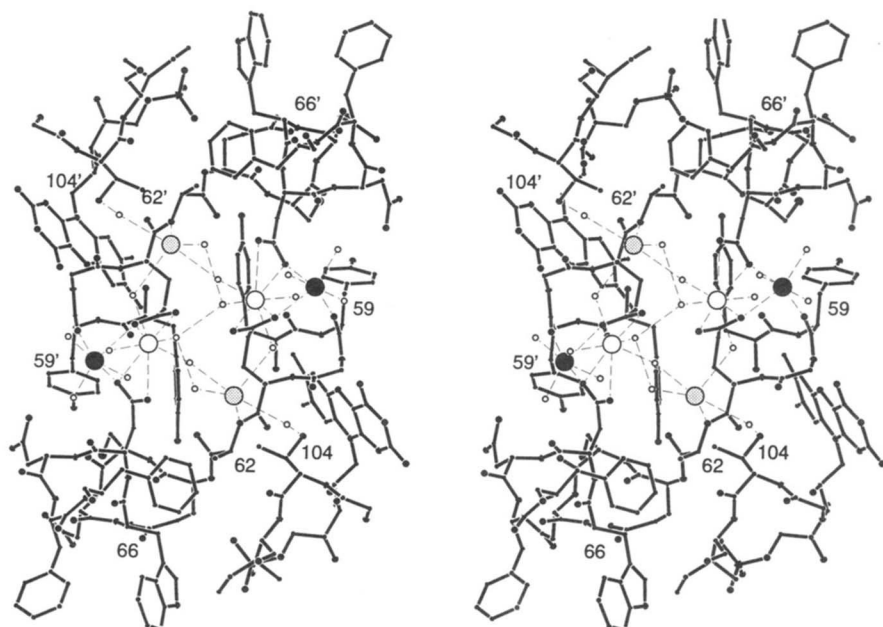


**Fig. 5.** Ion and water cluster that bridges molecules related by NCS in orthorhombic crystals. The view is along the local twofold axis. There are very few direct intermolecular contacts between protein atoms; most contacts are mediated by through-water bonds. Calcium ions are shown as large filled spheres, sodiums are shown as large open spheres, chlorides are shown as large grey spheres, and water molecules as small open spheres. Dashed lines represent polar contacts between atoms. The drawing was prepared with the program MAXIM, written by M. Rould.

ized flavodoxin from *Azotobacter* lacks biological activity (Yoch, 1975), suggesting that the dimerization blocks formation of the transient complexes that are involved in electron transfer.

#### Surface features and interactions of *E. coli* flavodoxin with methionine synthase

Examination of the surfaces that come into contact when dissociable protein–protein complexes form (Janin & Chothia, 1990; Jones & Thornton, 1996) shows a distribution of residues not very different from that found in protein surfaces in general, where hydrophobic residues constitute about 55% of the accessible surface area (Janin & Chothia, 1990). Hydrogen bonds, often involving charged partners, stabilize these protein–protein complexes, and waters may bridge polar groups. The matching of hydrophobic patches or interpenetration of hydrophobic residues is less frequent than in domain–domain interfaces (Jones & Thornton, 1996). Interfaces in the structures of two electron transfer complexes, cytochrome *c*–cytochrome *c* peroxidase (Pelletier & Kraut, 1992) and amicyanin–methylamine dehydrogenase (Chen et al., 1992), reveal a mixture of hydrogen bonding interactions, other polar contacts, and apolar contacts, as expected. In the amicyanin–methylamine dehydrogenase complex, a ring of hydrophobic residues from amicyanin encircles one of the copper ligands and participates in the interface.

To identify the residues most likely to be crucial for selective binding and for formation of functional complexes of *E. coli* flavodoxin and methionine synthase, we have examined molecular surfaces in the vicinity of the flavin, comparing the long-chain flavodoxins from *E. coli*, *Anabaena* 7120, *Synechococcus* 7942,

and *H. influenzae* (Fig. 3). Except for the flavodoxin from *H. influenzae*, the X-ray structures of these proteins are known, permitting detailed comparisons of surface shapes and electrostatic potentials that may provide clues to the species discrimination displayed in the interaction of flavodoxins with methionine synthase (Fig. 6). Differences in backbone conformation between *E. coli* and *Synechococcus* or *Anabaena* flavodoxins are very small in all of the chain segments displayed in Figure 6, with RMS values of 0.75 and 0.74 Å, respectively. Thus, the properties of side chains appear to be the major determinants of the selective recognition of *E. coli* flavodoxin. Residue charges, residue shape and surface accessibility, and sequence conservation suggest a subset of residues on the surface surrounding the flavin as candidates for further study (Table 3). The selection of critical residues included comparisons of the sequences of *E. coli* and *H. influenzae* flavodoxins. Because sequences of methionine synthase and PFL from *H. influenzae* are very similar to sequences of the corresponding *E. coli* proteins, residues common to *E. coli* and *H. influenzae* flavodoxins may be important in binding to the electron acceptors of activation systems.

Figure 6 compares some of the surface residues of *E. coli* and *Synechococcus* flavodoxins that are within 20 Å of the dimethylbenzene end of the flavin ring, and includes the residues listed in Table 3. The protruding tyrosines at positions 58, 59, and 97 are prominent in this figure. All three tyrosines play important roles in protein–protein interactions in the crystals we have studied. Ala 62 in *E. coli* flavodoxin, which replaces Leu or Ile in the other sequences, may affect surface complementarity. The fitting of complementary shapes to avoid steric overlap is a primary criterion in successful docking of protein structures (Katchalski-Katzir et al., 1992).

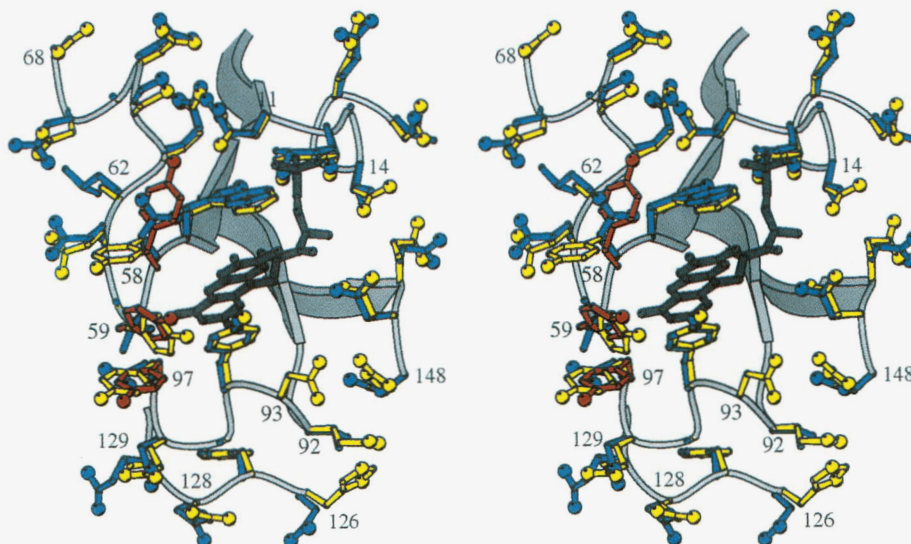


**Fig. 6.** Comparison of *E. coli* and *Synechococcus* flavodoxins. Residues that differ in the two flavodoxins are drawn in full-atom mode to show details of the changes in charge and size that affect the properties of the surfaces in the neighborhood of the flavin ring. Residues from *Synechococcus* flavodoxin are blue, those from the orthorhombic form of *E. coli* flavodoxin are yellow, and those from the trigonal form of *E. coli* flavodoxin are red. The drawing is centered at the dimethylbenzene moiety of the flavin because it is solvent accessible in flavodoxin and is close to other prosthetic groups that accept electrons in several complex flavoenzymes, including phthalate dioxygenase reductase, trimethylamine dehydrogenase, and cytochrome P450 reductase (Lim et al., 1986; Correll et al., 1992; Kim et al., 1997). However, this donor–acceptor orientation is not the only possible configuration for electron transfer from flavins; for example, in flavocytochrome *b*<sub>2</sub>, N(5) of the flavin is closest to the heme acceptor (Xia & Mathews, 1990).

**Table 3.** Important surface residues

Residue	Distance from flavin 8-methyl carbon (Å)	Contact surface (Å <sup>2</sup> ) <sup>a</sup>	Equivalent residue <sup>b</sup>
Tyr 58	11.8 (OH) <sup>c</sup>	54.7	Asn
Tyr 59	8.5 (OH)	34.4	Val, Thr, Ile
Ala 62	14.5 (CB)	1.2	Leu, Ile, Asp
Asp 68	18.3, 17.9 (OD1, OD2)	15.0	Gly
Glu 92	12.8, 13.9 (OE1, OE2)	20.4	Ile, Val
Asp 93	7.0, 9.0 (OD1, OD2)	26.7	Gly
Tyr 97	13.9 (OH)	23.9	Asn
Glu 128	17.5, 18.2 (OE1, OE2)	33.4	Asn
Arg 148	9.7, 8.1, 10.6 (NE, NH1, NH2)	23.2	Asn

<sup>a</sup>Exposed contact surface of all atoms in residue. The contact surface of each residue was determined using X-PLOR (Brünger, 1992) according to the definition in Lee and Richards (1971).

<sup>b</sup>The residue that appears in the same position in other long-chain flavodoxins.

<sup>c</sup>Atom used in calculating distance.

Asp 68, Glu 92, Asp 93, Glu 128, and Arg 148 of *E. coli* flavodoxin align with residues that are uncharged in *Anabaena* or *Synechococcus* flavodoxins (Figs. 3, 6), and could contribute to the selective recognition of *E. coli* flavodoxin by modulating electrostatic interactions. The formation of complexes of electron-transfer proteins has been found to depend on electrostatic interactions (DePascalis et al., 1993; Northrup et al., 1993; Guillemette et al., 1994). The binding constants and rates of formation of flavodoxin or ferredoxin complexes with ferredoxin reductase vary with ionic strength (Foust et al., 1969; Hurley et al., 1994), and the affinity of flavodoxin for methionine synthase decreases with ionic strength, as expected if favorable electrostatic interactions contribute to the free energy of binding (Hoover, 1997).

The protein that donates electrons to flavodoxin for activation of methionine synthase and other enzymes is *E. coli* flavodoxin-NADP<sup>+</sup>-reductase. The structures of FNR from *E. coli* (Ingelman et al., 1997) and FNR from *Anabaena* 7119 (Serre et al., 1996) have been reported recently, and the structural features that may control recognition and reaction rates in electron-transfer complexes of FNRs have been discussed (Hurley et al., 1995, 1996; Gomez-Moreno et al., 1996). Mutagenesis of *Anabaena* flavodoxins has shown several acidic residues in the regions corresponding to 123–129 and 145–147 of *E. coli* flavodoxin to be critical for the interaction with FNR from *Anabaena* (Medina et al., 1992). The structural similarities of flavodoxins and of flavodoxin reductases from *E. coli* and *Anabaena* (Bianchi et al., 1993b; Serre et al., 1996; Ingelman et al., 1997) make it very likely that the bottom right surface of *E. coli* flavodoxin, as viewed in Figure 6, is a region that interacts with FNR. Modeling of the interaction of *E. coli* flavodoxin reductase with *Anabaena* flavodoxin supports this conclusion (Ingelman et al., 1997).

We surmise that an overlapping region of the surface of *E. coli* flavodoxin, including some of the same residues that recognize FNR, interacts with methionine synthase. *E. coli* FNR competes with methionine synthase for *E. coli* flavodoxin; indeed, the competition has been exploited to measure the binding of flavodoxin to methionine synthase (Hoover et al., 1997). At the same time, incomplete correspondence of the surface(s) that contact FNR and

methionine synthase may allow for independent “tuning” of the relative binding specificities of each donor or acceptor. Recent studies of reactions of flavodoxins from *Anabaena* indicate that electron transfer may be controlled by different surface features of flavodoxin, depending on the acceptor. Site-directed mutations of *Anabaena* flavodoxin gave rise to different alterations of reactivities with the three electron acceptors, photosystem I, ferredoxin-NADP<sup>+</sup> reductase, and cytochrome *c* (Navarro et al., 1995).

Site-directed mutagenesis of the residues listed in Table 3 is in progress. The effects of mutation on the interactions with both FNR and methionine synthase should help to define the interfaces that are critical for each of these electron transfer reactions. However, structure analyses of complexes of flavodoxin with methionine synthase will be essential to establish the nature and extent of conformation changes that are induced by the binding of flavodoxin.

## Materials and methods

### Purification of *E. coli* flavodoxin

Flavodoxin was purified from strain DH01 using the IPTG-inducible overexpression plasmid DH1 (Bianchi et al., 1993a). The bacteria were typically grown in 3 liters of LB with 50 µg/mL ampicillin, shaking at 275 rpm at 37 °C until mid-log phase (OD<sub>460</sub> = 1.0), and protein expression was induced with IPTG at a final concentration of 100 µM. Two micrograms riboflavin were added along with the IPTG to compensate for depletion of FMN on overexpression of flavodoxin (Borruel et al., 1994). The bacteria were harvested 6–10 h later by centrifugation. The induction of the protein was apparent from the dark blue-grey color of the growing cells, indicative of high concentrations of the semiquinone form of flavodoxin. The cells were washed and resuspended in 50 mM Tris, 25 mM EDTA, pH 7.5, 2 µg/mL TLCK, 20 µg/mL PMSF, and 1/1,000 dilution of aprotinin, and lysed by French press. The unbroken cells and membranous fraction were separated by ultracentrifugation; the supernatant was diluted 1:3 with deionized water, and applied to a DEAE-FF Sepharose column (~75 mL) equilibrated with 50 mM Tris, pH 7.5, at 4 °C. After loading, the column was washed with one volume of 50 mM Tris, pH 7.5, and then with two column volumes of 100 mM NaOAc, pH 5.0. The protein was eluted with a 500-mL gradient of 100–500 mM NaCl in 100 mM NaOAc, pH 5.0. This step removes the major contaminant of flavodoxin, DNA (Vetter & Knappe, 1971). Immediately after collection, the orange fractions were adjusted to neutral pH by adding 1 M Tris, pH 8.0, to prevent the dissociation of FMN from the protein at low pH. The fractions were pooled, concentrated, and dialyzed against 50 mM Tris, pH 7.5, and the protein was loaded onto an HR16/10 monoQ FPLC column (LKB Pharmacia, Uppsala) at room temperature. The column was washed with the same buffer, and flavodoxin was eluted with a gradient of 100–700 mM NaCl, 50 mM Tris, pH 7.5. The yields ranged from 10 to 15 mg per gram of wet cell paste. The protein was stored in 50 mM Bis-Tris, 1 mM EDTA, pH 7.0, at –80 °C. Protein concentrations were calculated from the absorbance of the bound FMN at 466 nm ( $\epsilon = 8,250 \text{ M}^{-1} \text{ cm}^{-1}$ ) (Vetter & Knappe, 1971). This extinction coefficient was verified by titration of free FMN with flavodoxin apoprotein (see below).

### Measurement of FMN binding to apoflavodoxin

Apoflavodoxin was prepared by precipitation with trichloroacetic acid (D'Anna & Tollin, 1972), and was stored in 100 mM potas-

sium phosphate, pH 7.0, 0.1 mM EDTA, and 50 mM DTT. Concentration of the apoprotein was determined by standard BCA colorimetric methods (Smith et al., 1985), as well as by reconstitution with FMN (95% pure by HPLC, a generous gift of Dr. Vincent Massey, the University of Michigan). One milliliter of 10  $\mu\text{M}$  FMN in 100 mM potassium phosphate, pH 7.0, was placed in a spectrophotometric cuvette and aliquots of apoflavodoxin were added while monitoring absorbance. In plots of concentration of apoflavodoxin versus  $A_{466}$ , a distinct breakpoint was seen when one equivalent of apoflavodoxin had been added to the FMN. At this point, the ratio of  $A_{274}/A_{466}$  was 5.8; this ratio was used as a check of protein purity. The extinction coefficient of FMN bound to flavodoxin could then be determined by the change of absorbance at 466 nm based on the known extinction coefficient for free FMN at pH 7.0.

The  $K_d$  for binding FMN to apoflavodoxin was determined by measuring the quenching of fluorescence of a 0.1  $\mu\text{M}$  solution of FMN on addition of apoflavodoxin (Mayhew, 1971). Because of the tight binding of FMN, a nonlinear form of the binding equation (Equation 2) was used to fit the measurements of % quenching versus total concentration of added apoflavodoxin (Hoover, 1997).

$$\alpha = \frac{\{[E] + [L] + K_d\} \pm \sqrt{\{[E] + [L] + K_d\}^2 - 4 \cdot [E] \cdot [L]}}{2 \cdot [E]} \quad (2)$$

where  $[E]$  is the total concentration of protein and  $[L]$  is the total concentration of ligand.

#### Crystallization

Small needles of the orthorhombic form grew at 4 °C in 30 mM Bis-Tris, pH 7.0, in the presence of 60 mM CaCl<sub>2</sub>, 0.01% lauryldimethylamineoxide, and 20% PEG 400. The crystals typically appeared in 7–10 days, and attained full size in 2 weeks. Larger crystals suitable for data collection were obtained using MPD as the precipitant. They were reproducibly grown by microseeding techniques, mixing 10  $\mu\text{L}$  of protein (15–20 mg/mL in 10 mM imidazole, pH 7.0) with 10  $\mu\text{L}$  microseed precipitant solution (40% MPD, 100 mM CaCl<sub>2</sub>, 20 mM Bis-Tris, 10 mM imidazole, pH 7.0, 22 °C) containing a 10<sup>5</sup>–10<sup>6</sup>-fold dilution of a microseed stock solution, and equilibrating the drops over 0.5–1.0 mL microseed precipitant solution for 2–4 days. The microseed stock was obtained by crushing the needles from several hanging drops in which crystals had grown in PEG 400, and diluting into 1 mL of microseed precipitant solution.

The crystals used in diffraction experiments grew to a size of 0.5 × 0.2 × 0.2 mm, and the useful resolution limit was 1.8 Å. The space group was determined to be P2<sub>1</sub>2<sub>1</sub>2<sub>1</sub>, with  $a = 126.82$ ,  $b = 41.53$ ,  $c = 69.48$  Å. The molecular volume,  $V_M$ , corresponding to two molecules per asymmetric unit, is 2.20 Å<sup>3</sup> Da<sup>-1</sup>. The expected solvent content would be 44.1%, assuming a value of 1.23 Å<sup>3</sup> Da<sup>-1</sup> for the protein specific volume (Matthews, 1968).

A trigonal crystal form was obtained in the absence of Bis-Tris, but was found to be merohedrally twinned. Superposition of the twin reciprocal lattices, P312 and P321, leads to apparent 622 symmetry. Data from highly twinned crystals could be indexed equally well in space groups P3, P312, P321, P6, and P622, with  $R_{\text{sym}}$  for P622 as low as 0.09. Twinning was initially suspected from the apparent high symmetry, because crystals of space group P622 with unit cell dimensions  $a = b = 79.26$  Å,  $c = 51.74$  Å and

12 molecules per cell would have a molecular volume of only 1.17 Å<sup>3</sup> Da<sup>-1</sup>, well below the empirical lower limit for protein crystals of 1.68 Å<sup>3</sup> Da<sup>-1</sup> (Matthews, 1968). The percentage twinning was determined from intensity statistics (Yeates, 1988) to range from 30 to 50%, which precluded detwinning the data analytically (Redinbo & Yeates, 1993).

Normally, the trigonal crystals grow as hexagonal rods or plates. However, in one or two hanging drops in which 8  $\mu\text{L}$  of 15 mg/mL protein was mixed with 8  $\mu\text{L}$  well solution (30% MPD, 100 mM CaCl<sub>2</sub>, 200 mM PIPES, pH 7.0, 22 °C), a few triangular plate-like untwinned crystals were obtained. The crystal used in this work was 0.2 mm along the triangular edge and 0.08 mm thick, and diffracted to 2.5 Å at 140 K. The space group was determined to be P312,  $a = b = 78.83$  Å,  $c = 52.07$  Å, with one molecule in the asymmetric unit ( $V_M = 2.3$  Å<sup>3</sup> Da<sup>-1</sup>, 46.5% solvent content).

#### Data collection

Crystals were mounted in capillaries for all X-ray diffraction experiments at 277 K. For cryocrystallography at 140 K, crystals were affixed to Kevlar loops mounted on aluminum posts. Before freezing, the crystals were first slowly exchanged into a holding solution containing 50% MPD in steps of 1–2%, waiting 30 min between each step to allow for equilibration. They were frozen in the cooling stream of N<sub>2</sub> gas (at ~110 K). All data were collected using a multiwire area detector from Area Detector Systems Corporation (Hamlin, 1985; Xuong et al., 1985) equipped with a Huber three-circle goniostat. The X-ray source was a Rigaku RU200 rotating anode X-ray generator, and the incident beam was reflected from a graphite monochromator. Complete data sets were collected from single crystals according to the strategy of Xuong et al. (1985). Data were retained for structure determination only if the decay in the outermost annulus of resolution was less than 25%. For data collected at 140 K, no significant decay was seen at any resolution. Data sets were processed and merged using SDMS software (Howard et al., 1985). Statistics are given in Table 4.

#### Molecular replacement

Because the amino acid sequences of the flavodoxins from *Synechococcus* 7942 and *E. coli* (Osborne et al., 1991) are so similar (48.9% identity), a polyalanine-glycine model derived from coordinates for *Synechococcus* 7942 flavodoxin (PDB 10fv) (Drennan, 1995) was used for molecular replacement and Patterson correlation refinement in X-PLOR (Brünger, 1992). Data for these com-

**Table 4.** X-ray data sets

Data set	Space group	Resolution (Å)	Equivalent reflections (% complete)	$R_{\text{sym}}^a$	Temp. (K)
ECFL09	P2 <sub>1</sub> 2 <sub>1</sub> 2 <sub>1</sub>	2.85	17,287/7,580 (82.1)	0.056	277
ECFL13	P2 <sub>1</sub> 2 <sub>1</sub> 2 <sub>1</sub>	2.4	48,799/13,365 (90.4)	0.068	277
ECFL20	P2 <sub>1</sub> 2 <sub>1</sub> 2 <sub>1</sub>	2.0	12,5778/22,766 (89.6)	0.082	277
ECFL25	P2 <sub>1</sub> 2 <sub>1</sub> 2 <sub>1</sub>	1.8	21,3264/32,752 (97.1)	0.072	140
ECFL30	P312	2.6	56,473/5,995 (96.8)	0.064	140

<sup>a</sup> $R_{\text{sym}} = \sum_{hkl} |I(hkl) - \bar{I}(hkl)| / \sum_{hkl} I(hkl)$ .

putations were collected at 4 °C (ECFL09 in Table 4). Various resolution ranges and vector lengths were applied in the calculation; the highest correlation values were found for data from 8 to 3.5 Å resolution and a Patterson vector range of 5 to 15 Å. Rigid-body Patterson correlation refinements were performed on the highest ~100 peaks from the rotation searches. The strongest peaks calculated by Patterson correlation refinements were independent of resolution range used in the calculation (Brünger, 1990).

Translation searches with the oriented models were performed using data from 8.0 to 3.5 Å resolution; the two independently positioned models were referred to a common origin by computing correlation coefficients with one molecule fixed and the other at one-half unit cell translations relative to its original position. Only one combination of model positions was seen to be stereochemically reasonable from examination of the overall packing after translation searches; for this arrangement, the  $R$  was 0.538 and the correlation coefficient was 0.399. The resolution was extended to 3.0 Å for rigid-body and initial least-squares minimizations (Brünger, 1992). At this stage, maps with coefficients ( $|F_o| - |F_c|$ ) showed well-connected density for the backbone, and ( $|F_o| + |F_c|$ ) maps revealed densities corresponding to the sulfurs of residues Cys 64 and Cys 99, which were both modeled as alanines, and to side chains of Phe 7, Phe 8, Trp 57, Trp 66, and Trp 120. After simulated annealing refinements in which the FMN group was omitted from the model, ( $|F_o| - |F_c|$ ) densities for the FMN group were obvious.

#### Refinement of the orthorhombic form of *E. coli* flavodoxin

Refinement was conducted in a series of stages (Table 5), each of which began with inspection and rebuilding or addition of atoms to

the model, guided by electron density maps and difference electron density maps typically computed with  $\sigma_A$ -weighted coefficients (Read, 1986). The new model was then subjected to overall  $B$ -factor refinement, conjugate-gradient positional refinement, and slow-cooling simulated annealing (2,000 °C to 300 °C in 25° steps) (Brünger & Kruckowski, 1990). After annealing, positions and temperature factors were again refined. In the early stages, the initial polyalanine model was replaced with the correct sequence for *E. coli* flavodoxin, and refined at 3.0 Å resolution versus the data set ECFL09, collected at 4 °C, to an  $R$  of 0.199. The model was then refined against data extending to 2.4 Å resolution that had been collected at 4 °C (ECFL13). Omit maps calculated with coefficients ( $|F_o| - |F_c|$ ) showed several intense peaks and another connected region that could not be protein, and these were modeled as calcium ions and a Bis-Tris molecule. Parameters for the Bis-Tris molecule were approximated using average values from small organic molecule structures. The  $R$  for the 2.4-Å structure (including 91 waters, three calciums, and one Bis-Tris molecule) was 0.193. The model was further refined to 2.0 Å using data collected at 4 °C from a third crystal (ECFL20), giving an  $R$  of 0.237.

In subsequent refinements using data collected at 140 K (ECFL25), additional water molecules and ions were seen coordinated to protein or solvent atoms. Solvents were added if they appeared as peaks  $\geq 3\sigma$  in ( $|F_o| - |F_c|$ ) maps and made reasonable hydrogen bonds with other atoms. During these refinements, ( $|F_o| - |F_c|$ ) maps revealed a second Bis-Tris/calcium complex, and altogether four calciums, two Bis-Tris molecules, four sodiums, and two chlorides were modeled into the density (see below). In the later stages of refinement at 1.8 Å resolution, NCS restraints were removed. Overall anisotropic temperature factor corrections

**Table 5.** Model building and refinement

Data set	Stage	Number of atoms (non-hydrogen)		Resolution range (Å)	Unique reflections	$R_{initial}^a$	$R_{final}$
		Protein & FMN	sol/BT/Ca/Na/Cl				
ECFL09	1	1,132	0/0/0/0/0	8.0–3.0	6,196	0.523	0.406
	5	2,797	0/0/0/0/0	15.0–3.0	6,570	0.268	0.199
ECFL13	1	2,797	0/0/0/0/0	8.0–2.5	11,249	0.296	0.230
	6	2,832	44/14/2/0/0	8.0–2.5	11,249	0.197	0.189
	12	2,832	97/14/2/0/0	8.0–2.4	12,314	0.286	0.210
	21	2,832	91/14/3/0/0	15.0–2.4	12,938	0.201	0.193
ECFL20	1	2,832	0/0/0/0/0	8.0–2.0	20,948	0.305	0.270
	3	2,832	93/14/3/0/0	20.0–2.0	21,328	0.248	0.237
ECFL25	1	2,832	0/0/0/0/0	8.0–2.4	13,462	0.511	0.303
	2	2,832	60/14/3/0/0	8.0–2.4	13,462	0.311	0.229
	5	2,832	283/14/3/0/0	8.0–2.0	23,082	0.231	0.213
		2,832	450/14/3/0/0	8.0–1.8	30,934	0.223	0.212
	15	2,832	403/28/4/4/2	10.0–1.8	30,211	0.197	0.189
	19 <sup>b</sup>	2,832	354/28/4/4/2	10.0–1.8	32,072	0.202	0.196
	1	1,367	0/0/0/0/0	6.0–3.0	3,603	0.416	0.336
ECFL30 <sup>c</sup>	5 <sup>b</sup>	1,367	55/0/1/0/0	10.0–2.6	5,702	0.195	0.191

<sup>a</sup> $R = \sum_{hkl} |F_o(hkl)| - |F_c(hkl)| / |\sum_{hkl} F_o(hkl)|$ , for all reflections.

<sup>b</sup>Refinement with no intensity cutoff ( $I > 0$ ).

<sup>c</sup>Data from the trigonal crystal form.

**Table 6.** Crystal data and refinement statistics (140 K)

	Orthorhombic	Trigonal
Space group	P2 <sub>1</sub> 2 <sub>1</sub> 2 <sub>1</sub>	P312
Cell constants (Å)		
<i>a</i>	126.40	78.83
<i>b</i>	41.10	78.83
<i>c</i>	69.15	52.07
Resolution (Å)	10.0–1.8	10.0–2.6
Reflections (measured/unique)	213,264/32,752	56,473/5,995
Completeness (overall/last bin, %)	97.1/93.4 (1.94–1.8)	99.4/98.1 (2.7–2.6)
<i>R</i> <sub>sym</sub> <sup>a</sup> (overall/last bin)	0.072/0.166	0.064/0.190
<i>I</i> / <i>σ</i> ( <i>I</i> ) (overall/last bin)	26.3/5.9	17.4/3.8
<i>R</i> <sub>work</sub> <sup>b</sup> / <i>R</i> <sub>free</sub> <sup>c</sup>	0.196/0.250	0.191/0.249
Estimated coordinate error <sup>d</sup> (Å)	0.19	0.25
RMSD: bonds (Å)	0.009	0.012
RMSD: angles (degrees)	1.5	1.3
<i>B</i> (Å <sup>2</sup> )	22.7 <sup>e</sup>	21.0

<sup>a</sup>*R*<sub>sym</sub> =  $\sum_{hkl} |I(hkl) - \langle I(hkl) \rangle| / \sum_{hkl} \langle I(hkl) \rangle$ .

<sup>b</sup>*R*<sub>work</sub> =  $\sum_{hkl} |F_o(hkl)| - |F_c(hkl)| / \sum_{hkl} |F_o(hkl)|$ , for reflections with *I* > 0, that were used in refinement.

<sup>c</sup>*R*<sub>free</sub> =  $\sum_{(hkl) \in T} |F_o(hkl)| - |F_c(hkl)| / \sum_{(hkl) \in T} |F_o(hkl)|$ , where *T* is a randomly chosen set of reflections (approximately 10% of the data) not used during refinement (Brünger, 1993).

<sup>d</sup>(Luzzati, 1952).

<sup>e</sup>Excluding residues 171–176 in each molecule.

were applied, and bulk solvent corrections were included as described in Jiang and Brünger (1994), using X-PLOR 3.8. In the final refinements leading to stage 19, all data with *I* > 0 were used and were divided into test and working sets for calculation of *R*<sub>free</sub>. Most solvents refined with *B*-factors slightly above the average *B*-factor of the protein (22.7 Å<sup>2</sup>), but a few had *B*-factors of 40 Å<sup>2</sup> or larger. Putative solvent molecules were eliminated from the model if their scattering contributions were <20% of an oxygen atom at rest and at full occupancy or if they were not within 3.6 Å of suitable donors or acceptors. At the conclusion of stage 19, the *R*<sub>work</sub> was 0.196 for data between 10.0 and 1.8 Å and *R*<sub>free</sub> was 0.250 (Table 6). Corresponding *R* values for data with *I* > 2*σ*(*I*) were 0.193 and 0.246. The parameters from this refinement were deposited in the PDB, with filecode 1ag9.

#### Modeling of calcium and other ions in the orthorhombic structure

The parameters for refinement of the calcium ions were derived from several well-refined structures in the PDB, and an average distance of Ca···O was set at 2.34 Å. In maps calculated with data collected at low temperature and 1.8 Å resolution, several additional peaks were found that could not be modeled satisfactorily as water molecules. Two chloride and four sodium ions were modeled into these sites; the validity of these ion assignments was indicated by the lack of positive and negative density ripples, which would arise if the number of electrons modeled were not appropriate, as well as the ion···ligand distances, which refined well to the expected values (Na···O = 2.45 Å, Cl···O = 3.00 Å).

#### Refinement of the trigonal form of *E. coli* flavodoxin

The trigonal structure (data set ECFL30) was solved by molecular replacement, using the refined orthorhombic structure. The rota-

tion function gave a clear, single peak 5.4 *σ* above the average at θ<sub>1</sub> = 155, θ<sub>2</sub> = 40, θ<sub>3</sub> = 40 (Eulerian angles) for data between 8.0 and 4.0 Å. The translation function also gave a clear peak at 8.9 *σ* above the average (correlation coefficient, 0.473), with the next peak at 7.5 *σ* (correlation coefficient, 0.423). After a rigid-body refinement against data from 8.0 to 3.0 Å, the *R* decreased to 0.336. A single cycle of simulated annealing reduced *R*<sub>work</sub> to 0.193, and *R*<sub>free</sub> to 0.282. Overall anisotropic temperature factor corrections were applied, and a bulk solvent correction, as implemented in X-PLOR 3.1, was included to extend the inner resolution to 10.0 Å. After five rounds of refinement, in which rebuilding of side chains and the addition of waters and one calcium ion were alternated with simulated annealing, positional, and overall and individual *B*-factor refinement, the *R* was 0.191 and *R*<sub>free</sub> was 0.249. Several solvents occupy special positions on two- or three-fold axes; some of these solvents may be Na<sup>+</sup> rather than water. Residues 171–176 could not be placed in density and have been omitted from the model. The PDB filecode for the trigonal form of *E. coli* flavodoxin is 1ahn.

#### Acknowledgments

We thank Drs. Rowena Matthews and Vincent Massey, who made facilities in their laboratories available for growth of *E. coli*, protein purification, and spectrophotometric and fluorescence titrations. We are grateful to Dr. Matthews and to Drs. M.M. Dixon, J.J. Jarrett, and C. Goulding for comments and discussions, and to Anita Metzger for assistance with the final rounds of refinement. This research was supported by a grant from the National Institutes of Health (GM 16429).

#### References

- Banerjee RV, Harder SR, Ragsdale SW, Matthews RG. 1990. Mechanism of reductive activation of cobalamin-dependent methionine synthase: An electron paramagnetic resonance spectroelectrochemical study. *Biochemistry* 29:1129–1135.

- Bianchi V, Eliasson R, Fontecave M, Mulliez E, Hoover DM, Matthews RG, Reichard P. 1993a. Flavodoxin is required for the activation of the anaerobic ribonucleotide reductase. *Biochem Biophys Res Commun* 197:792–797.
- Bianchi V, Reichard P, Eliasson R, Pontis E, Krook M, Jörnvall H, Häggard-Ljungquist E. 1993b. *E. coli* ferredoxin NADP<sup>+</sup> reductase: Activation of *E. coli* anaerobic ribonucleotide reduction, cloning of the gene (*fpr*) and overexpression of the protein. *J Bacteriol* 175:1590–1595.
- Birch OM, Fuhrmann M, Shaw NM. 1995. Biotin synthase from *Escherichia coli*, an investigation of the low molecular weight and protein components required for activity in vitro. *J Biol Chem* 270:19158–19165.
- Blaschkowski HP, Neuer G, Ludwig-Festl M, Knappe J. 1982. Routes of flavodoxin and ferredoxin reduction in *Escherichia coli*. CoA-acylating pyruvate: Flavodoxin and NADPH:flavodoxin oxidoreductases participating in the activation of pyruvate formate-lyase. *Eur J Biochem* 123:563–569.
- Borruel A, Peleato ML, Orera VM, Gomez-Moreno C, Fillat MF. 1994. Electron paramagnetic resonance as a tool for monitoring overexpression in *Escherichia coli* of fully functional flavodoxin. *Anal Biochem* 218:255–258.
- Brünger AT. 1990. Extension of molecular replacement: A new search strategy based on Patterson correlation refinement. *Acta Crystallogr A* 46:46–57.
- Brünger AT. 1992. *X-PLOR version 3.1. A system for X-ray crystallography and NMR*. New Haven: Yale University Press.
- Brünger AT. 1993. Assessment of phase accuracy by cross validation: The free R-value, methods and applications. *Acta Crystallogr D* 49:24–36.
- Brünger AT, Kruckowski A. 1990. Slow-cooling protocols for crystallographic refinement by simulated annealing. *Acta Crystallogr A* 46:585–593.
- Burkhart BM, Ramakrishnan B, Hongao Y, Reedstrom RJ, Markley JL, Straus NA, Sundaralingam M. 1995. Structure of the trigonal form of recombinant oxidized flavodoxin from *Anabaena* 7120 at 1.40 Å resolution. *Acta Crystallogr D* 51:318–330.
- Burnett RM, Darling GD, Kendall DS, LeQuesne ME, Mayhew SG, Smith WW, Ludwig ML. 1974. The structure of the oxidized form of clostridial flavodoxin at 1.9 Å resolution. *J Biol Chem* 249:4383–4392.
- Chen L, Durley R, Poliks BJ, Hamada K, Chen Z, Mathews FS, Davidson VL, Satow Y, Huizinga E, Velleix FMD, Hol WGJ. 1992. Crystal structure of an electron-transfer complex between methylamine dehydrogenase and amicyanin. *Biochemistry* 31:4959–4964.
- Correll CC, Batie JC, Ballou DP, Ludwig ML. 1992. Phthalate dioxygenase reductase: A modular structure for electron transfer from pyridine nucleotides to [2Fe-2S]. *Science* 258:1604–1610.
- D'Anna JA, Tollin G. 1972. Studies of flavin-protein interaction in flavoproteins using protein fluorescence and circular dichroism. *Biochemistry* 11:1073–1080.
- Deistung J, Cannon FC, Cannon MC, Hill S, Thorneley RN. 1985. Electron transfer to nitrogenase in *Klebsiella pneumoniae*. *nifF* gene cloned and the gene product, a flavodoxin, purified. *Biochem J* 231:743–753.
- DePascalis AR, Jelesarov I, Ackermann F, Koppenol WH, Hirashima M, Knaff DB, Bosshard HR. 1993. Binding of ferredoxin to ferredoxin:NADP<sup>+</sup> oxidoreductase: The role of carboxyl groups, electrostatic surface potential, and molecular dipole moment. *Protein Sci* 2:1126–1135.
- Draper RD, Ingram LL. 1968. A potentiometric study of the flavin semiquinone equilibrium. *Arch Biochem Biophys* 125:802–808.
- Drennan CL. 1995. Crystallographic studies of FMN and vitamin B<sub>12</sub> dependent enzymes: Flavodoxin and methionine synthase. PhD Dissertation. Ann Arbor, Michigan: The University of Michigan.
- Drennan CL, Dixon MM, Hoover DM, Jarrett JJ, Goulding CW, Mathews RG, Ludwig ML. 1997. In: Kräutler B, ed. *Vitamin B<sub>12</sub> and B<sub>12</sub> proteins*. Weinheim, Germany: Verlag Chemie. Forthcoming.
- Fillat MF, Sandmann G, Gómez-Moreno C. 1988. Isolation and characterization of flavodoxin from *Anabaena*. *Arch Microbiol* 150:160–164.
- Fleischmann RD, Adams MD, White O, Clayton RA, Kirkness EF, Kerlavage AR, Bult CJ, Tomb JF, Dougherty BA, Merrick JM, McKenney K, Sutton G, FitzHugh W, Fields C, Gocayne JD, Scott J, Shirley R, Liu LI, Glodek A, Kelley JM, Weidman JF, Philips CA, Spriggs T, Hedblom E, Cotton MD, Utterback TR, Hanna MC, Nguyen DT, Saudek DM, Brandon RC, Fine LD, Fritchman JL, Furhmann JL, Geoghegan NSM, Gnehm CL, McDonald LA, Small KV, Fraser CM, Smith HO, Venter JC. 1995. Whole-genome random sequencing and assembly of *Haemophilus influenzae* Rd. *Science* 269:496–512.
- Foust GP, Mayhew SG, Massey V. 1969. Complex formation between ferredoxin triphosphopyridine nucleotide reductase and electron transfer proteins. *J Biol Chem* 244:964–970.
- Franken H-P, Ruterjans H, Müller F. 1984. Nuclear-magnetic-resonance investigation of <sup>15</sup>N-labeled flavins, free and bound to *Megashaera elsdenii* apoflavodoxin. *Eur J Biochem* 138:481–489.
- Fujii K, Galvan JH, Huennekens FM. 1977. Activation of methionine synthase: Further characterization of the flavoprotein system. *Arch Biochem Biophys* 178:662–670.
- Fujii K, Huennekens FM. 1974. Activation of methionine synthetase by a reduced triphosphopyridine nucleotide-dependent flavoprotein system. *J Biol Chem* 249:6745–6753.
- Fukuyama K, Wakabayashi S, Matsubara H, Rogers LJ. 1990. Tertiary structure of oxidized flavodoxin from an eukaryotic red alga *Chondrus crispus* at 2.35 Å resolution. *J Biol Chem* 265:15804–15812.
- Gangeshwaran R, Eady RR. 1996. Flavodoxin 1 of *Azotobacter vinelandii*: Characterization and role in electron donation to purified assimilatory nitrate reductase. *Biochem J* 317:103–108.
- Gomez-Moreno C, Martinez-Julvez M, Fillat MF, Hurley JK, Tollin G. 1996. Molecular recognition in protein complexes involved in electron transfer. *Biochem Soc Trans* 24:111–116.
- Good NE, Winget GD, Winter W, Connolly TN, Izawa S, Singh RM. 1966. Hydrogen ion buffers for biological research. *Biochemistry* 5:467–477.
- Guillemette J, Barker P, Eltis L, Lo T, Smith M, Brayer G, Mauk AG. 1994. Analysis of the bimolecular reduction of ferricytochrome c by ferrocyanochrome b<sub>5</sub> through mutagenesis and molecular modelling. *Biochimie* 76:592–604.
- Hamlin R. 1985. Multiwire area X-ray diffractometers. *Methods Enzymol* 114:416–452.
- Havel TF. 1993. Predicting the structure of the flavodoxin from *Escherichia coli* by homology modeling, distance geometry and molecular dynamics. *Mol Simul* 10:175–210.
- Hoover DM. 1997. Thermodynamic and structural studies of flavodoxin and methionine synthase from *Escherichia coli*. PhD Dissertation. Ann Arbor, Michigan: The University of Michigan.
- Hoover DM, Jarrett JT, Sands RH, Dunham WR, Matthews RG, Ludwig ML. 1997. Interaction of *E. coli* cobalamin-dependent methionine synthase and its physiological partner flavodoxin: Characterization of conformational and thermodynamic changes in methionine synthase caused by the binding of flavodoxin. *Biochemistry* 36:127–138.
- Howard AJ, Nielsen C, Xuong NH. 1985. Software for a diffractometer with multiwire area detector. *Methods Enzymol* 114:452–472.
- Huang S, Mathews RG. 1997. Evidence for conformational changes associated with mutations of B<sub>12</sub>-dependent methionine synthase. *FASEB J* 11: A900.
- Hurley JK, Fillat M, Gomez-Moreno C, Tollin G. 1995. Structure-function relationships in the ferredoxin/ferredoxin:NADP<sup>+</sup> reductase system from *Anabaena*. *Biochimie* 77:539–548.
- Hurley JK, Medina M, Gomez-Moreno C, Tollin G. 1994. Further characterization by site-directed mutagenesis of the protein–protein interface in the ferredoxin/ferredoxin-NADP(+) reductase system from *Anabaena*—Requirement of a negative charge at position-94 in ferredoxin for rapid electron-transfer. *Arch Biochem Biophys* 312:480–486.
- Hurley JK, Schmeits JL, Genzor C, Gomez-Moreno C, Tollin G. 1996. Charge reversal mutations in a conserved acidic patch in *Anabaena* ferredoxin can attenuate or enhance electron transfer to ferredoxin:NADP<sup>+</sup> reductase by altering protein/protein orientation within the intermediate complex. *Arch Biochem Biophys* 333:243–250.
- Ifuku O, Koga N, Haze S, Kishimoto J, Wachi Y. 1994. Flavodoxin is required for conversion of dethiobiotin to biotin in *Escherichia coli*. *Eur J Biochem* 224:173–178.
- Ingleman M, Bianchi V, Eklund H. 1997. The three-dimensional structure of flavodoxin reductase from *Escherichia coli* at 1.7 Å resolution. *J Mol Biol* 268:147–157.
- Janin J, Chothia C. 1990. The structure of protein–protein recognition sites. *J Biol Chem* 265:16027–16030.
- Jarrett JT, Amarasinghe M, Drennan CT, Scholten JD, Sands RH, Ludwig ML, Mathews RG. 1996. Mutations in the B<sub>12</sub>-binding region of methionine synthase: How the protein controls methylcobalamin reactivity. *Biochemistry* 35:2464–2475.
- Jiang JS, Brünger AT. 1994. Protein hydration observed by X-ray diffraction. Solvation properties of penicillopepsin and neuraminidase crystal structures. *J Mol Biol* 264:100–115.
- Jones S, Thornton JM. 1996. Principles of protein–protein interactions. *Proc Natl Acad Sci USA* 93:13–20.
- Kabsch W, Sander C. 1983. Dictionary of protein secondary structure: Pattern recognition of hydrogen bonded and geometrical features. *Biopolymers* 22:2577–2637.
- Katchalski-Katzir E, Shariv I, Eisenstein M, Friesem AA, Aflalo C, Vakser IA. 1992. Molecular surface recognition: Determination of geometric fit between proteins and their ligands by correlation techniques. *Proc Natl Acad Sci USA* 89:2195–2199.
- Kim JJP, Wang M, Roberts DL, Paschke R, Shea T, Masters BSS. 1997. How do two flavins talk to each other? The three dimensional structure of rat liver NADPH-cytochrome P450 reductase. In: Stevenson KJ, Massey V, Williams CH Jr, eds. *Flavins and flavoproteins 1996*. Calgary, Alberta: University of Calgary Press. pp 455–461.

- Klugkist J, Voorberg J, Haaker H, Veeger C. 1986. Characterization of three different flavodoxins from *Azotobacter vinelandii*. *Eur J Biochem* 155:33–40.
- Kraulis PJ. 1991. MOLSCRIPT: A program to produce both detailed and schematic plots of protein structures. *J Appl Crystallogr* 24:946–950.
- Krey GD, Vanin EF, Swenson RP. 1988. Cloning, nucleotide sequence, and expression of the flavodoxin gene from *Desulfovibrio vulgaris* (Hildenborough). *J Biol Chem* 263:15436–15443.
- Laudenbach DE, Reith ME, Straus NA. 1988. Isolation, sequence analysis, and transcriptional studies of the flavodoxin gene from *Anacystis nidulans* R2. *J Bacteriol* 170:258–265.
- Lee B, Richards FM. 1971. The interpretation of protein structures: Estimation of static accessibility. *J Mol Biol* 55:379–400.
- Lim LW, Sharnala N, Mathews FS, Steenkamp DJ, Hamlin R, Xuong NH. 1986. Three-dimensional structure of the iron-sulfur flavoprotein trimethylamine dehydrogenase at 2.4 Å resolution. *J Biol Chem* 261:15140–15146.
- Ludwig ML, Luschinsky CL. 1992. Structure and redox properties of clostridial flavodoxin. In: Müller F, ed. *Chemistry and biochemistry of flavoenzymes III*. Boca Raton, Florida: CRC Press. pp 427–466.
- Ludwig ML, Matthews RG. 1997. Structure-based perspectives on B<sub>12</sub>-dependent enzymes. *Annu Rev Biochem* 66:269–311.
- Ludwig ML, Patridge KA, Metzger AL, Dixon MM, Eren M, Feng Y, Swenson RP. 1997. Control of oxidation-reduction potentials in flavodoxin from *Clostridium beijerinckii*: The role of conformation changes. *Biochemistry* 36:1259–1280.
- Ludwig ML, Schopfer LM, Metzger AL, Patridge KA, Massey V. 1990. Structure and oxidation-reduction behavior of 1-deaza-FMN flavodoxins: Modulation of redox potentials in flavodoxins. *Biochemistry* 29:10364–10375.
- Luzzati PV. 1952. Traitement statistique des erreurs dans la détermination des structures cristallines. *Acta Crystallogr* 5:802–810.
- Matthews BW. 1968. Solvent content of protein crystals. *J Mol Biol* 33:491–497.
- Mayhew SG. 1971. Studies on flavin binding in flavodoxins. *Biochim Biophys Acta* 235:289–302.
- Mayhew SG, Ludwig ML. 1975. Flavodoxins and electron-transferring flavoproteins. In: Boyer PD, ed. *The enzymes XII*. New York: Academic Press. pp 57–118.
- Mayhew SG, O'Connell DP, O'Farrell PA, Yalloway GN, Geoghegan SM. 1996. Regulation of the redox potentials of flavodoxins: Modification of the flavin binding site. *Biochem Soc Trans* 24:122–127.
- Mayhew SG, Tolin G. 1992. General properties of flavodoxins. In: Müller F, ed. *Chemistry and biochemistry of flavoenzymes III*. Boca Raton, Florida: CRC Press. pp 389–426.
- Medina M, Peleato ML, Mendez E, Gomez-Moreno C. 1992. Identification of specific carboxyl groups on *Anabaena* PCC 7119 flavodoxin which are involved in the interaction with ferredoxin-NADP<sup>+</sup> reductase. *Eur J Biochem* 203:373–379.
- Navarro JA, Hervas M, Genzor CG, Cheddar G, Fillat MF, de la Rosa MA, Gomez-Moreno C, Cheng H, Xia B, Chae YK, Yan H, Wong B, Straus NA, Markley JL, Hurley JK, Tolin G. 1995. Site-specific mutagenesis demonstrates that the structural requirements for efficient electron transfer in *Anabaena* ferredoxin and flavodoxin are highly dependent on the reaction partner: Kinetic studies with photosystem I, ferredoxin:NADP<sup>+</sup> reductase, and cytochrome c. *Arch Biochem Biophys* 324:229–238.
- Nieva-Gomez D, Roberts GP, Kevickis S, Brill WJ. 1980. Electron transport to nitrogenase in *Klebsiella pneumoniae*. *Proc Natl Acad Sci USA* 77:2555–2558.
- Northrup SH, Thomasson KA, Miller CM, Barker PD, Eltis LD, Guillemette JG, Inglis SC, Mauk AG. 1993. Effects of charged amino acid mutations on the bimolecular kinetics of reduction of yeast iso-1-ferredicytochrome c by bovine ferrocyanochrome b<sub>5</sub>. *Biochemistry* 32:6613–6623.
- Ollagnier S, Mulliez E, Schmidt RR, Eliasson R, Gaillard J, Deronzier C, Bergman T, Gräslund A, Reichard P, Fontecave M. 1997. Activation of the anaerobic ribonucleotide reductase from *Escherichia coli*. *J Biol Chem* 272:24216–24223.
- Osborne C, Chen LM, Matthews RG. 1991. Isolation, cloning, mapping, and nucleotide sequencing of the gene encoding flavodoxin in *Escherichia coli*. *J Bacteriol* 173:1729–1737.
- Pelletier H, Kraut J. 1992. Crystal structure of a complex between electron transfer partners, cytochrome c peroxidase and cytochrome c. *Science* 258:1748–1755.
- Ponstingl H, Otting G. 1997. NMR assignments, secondary structure and hydration of oxidized *Escherichia coli* flavodoxin. *Eur J Biochem* 244:384–399.
- Read R. 1986. Improved Fourier coefficients for maps using phases from partial structures with errors. *Acta Crystallogr A* 42:140–149.
- Redinbo MR, Yeates TO. 1993. Structure determination of plastocyanin from a specimen with a hemihedral twinning fraction of one-half. *Acta Crystallogr D* 49:375–380.
- Sanyal I, Gibson KJ, Flint DH. 1996. *Escherichia coli* biotin synthase: An investigation into the factors required for its activity and its sulfur donor. *Arch Biochem Biophys* 326:48–56.
- Serre L, Vellieux FMD, Medina M, Gomez-Moreno C, Fontecilla-Camps JC, Frey M. 1996. X-ray structure of the ferredoxin:NADP<sup>+</sup> reductase for the cyanobacterium *Anabaena* PCC 7119 at 1.8 Å resolution, and crystallographic studies of NADP<sup>+</sup> binding at 2.25 Å resolution. *J Mol Biol* 263:20–39.
- Shah VK, Stacey G, Brill WJ. 1983. Electron transport to nitrogenase. Purification and characterisation of pyruvate-flavodoxin oxidoreductase, the nifJ product. *J Biol Chem* 258:12064–12068.
- Smith PK, Krohn RI, Hermanson GT, Mallia AK, Gartner FH, Provenzano MD, Fujimoto EK, Goede NM, Olson BJ, Kleink DC. 1985. Measurement of protein using bicinchoninic acid. *Anal Biochem* 150:76–85.
- Smith WW, Patridge KA, Ludwig ML, Petsko GA, Tsernoglou D, Tanaka M, Yasunobu KT. 1983. Structure of oxidized flavodoxin from *Anacystis nidulans*. *J Mol Biol* 165:737–753.
- Stockman BJ, Westler WM, Mooberry ES, Markley JL. 1988. Flavodoxin from *Anabaena* 7120: Uniform nitrogen-15 enrichment and hydrogen-1, nitrogen-15, and phosphorus-31 NMR investigations of the flavin mononucleotide binding site in the reduced and oxidized states. *Biochemistry* 27:136–142.
- Sun X, Eliasson R, Pontis E, Andersson J, Buist G, Sjöberg BM, Reichard P. 1995. Generation of the glycyl radical of the anaerobic *Escherichia coli* ribonucleotide reductase requires a specific activating enzyme. *J Biol Chem* 270:2443–2446.
- Swenson RP, Krey GD. 1994. Site-directed mutagenesis of tyrosine-98 in the flavodoxin from *Desulfovibrio vulgaris* (Hildenborough): Regulation of oxidation-reduction properties of the bound FMN cofactor by aromatic, solvent, and electrostatic interactions. *Biochemistry* 33:8505–8514.
- Tanaka M, Hanu M, Yasunobu F, Mayhew SG. 1974. The amino acid sequence of the *Clostridium* MP flavodoxin. *J Biol Chem* 249:4393–4396.
- Thorne RNF, Deistung J. 1988. Electron-transfer studies involving flavodoxin and a natural redox partner, the iron protein of nitrogenase. *Biochem J* 253:587–595.
- Vetter HJ, Knappe J. 1971. Flavodoxin and ferredoxin of *Escherichia coli*. *Hoppe-Seyler's Z Physiol Chem* 352:433–446.
- Wakabayashi S, Kimura T, Fukuyama K, Matsubara H, Rogers LJ. 1989. The amino acid sequence of a flavodoxin from the eukaryotic red alga *Chondrus crispus*. *Biochem J* 263:981–984.
- Watengaugh KD, Sieker LC, Jensen LH. 1973. The binding of riboflavin-5'-phosphate in a flavoprotein: Flavodoxin at 2.0-Angstrom resolution. *Proc Natl Acad Sci USA* 70:3857–3860.
- Wong KK, Murray BW, Lewis SA, Baxter MK, Ridky TW, Uliassi-DeMario L, Kozařich JW. 1993. Molecular properties of pyruvate formate-lyase activating enzyme. *Biochemistry* 32:14102–14110.
- Xia Z, Mathews FS. 1990. Molecular structure of flavocytochrome b<sub>2</sub> at 2.4 Å resolution. *J Mol Biol* 212:837–863.
- Xuong NH, Nielsen C, Hamlin R, Anderson D. 1985. Strategy for data collection from protein crystals using a multiwire counter area detector diffractometer. *J Appl Crystallogr* 18:342–350.
- Yeates TO. 1988. Simple statistics for intensity data from twinned specimens. *Acta Crystallogr A* 44:142–144.
- Yoch DC. 1975. Dimerization of *Azotobacter vinelandii* flavodoxin (azotoflavin). *Arch Biochem Biophys* 170:326–333.
- Zhou Z, Swenson RP. 1995. Electrostatic effects of surface acidic amino acid residues on the oxidation-reduction potentials of the flavodoxin from *Desulfovibrio vulgaris* (Hildenborough). *Biochemistry* 34:3183–3192.
- Zhou Z, Swenson RP. 1996. The cumulative electrostatic effect of aromatic stacking interactions and the negative electrostatic environment of the flavin mononucleotide binding site is a major determinant of the reduction potential for the flavodoxin from *Desulfovibrio vulgaris* (Hildenborough). *Biochemistry* 35:15980–15988.